Improvement of the thermoelectric performance of boron-doped silicon by blocking minority carrier diffusion on the p^+/p interface

Sakamoto, Momoka
Chikushigaoka High School

Matsukawa, Yuko
Department of Materials, Kyushu University

Sasaoka, Rikuto
Department of Materials, Kyushu University

Minoshima, Kohei
Department of Materials, Kyushu University

他

出版情報：Japanese Journal of Applied Physics. 62 (7), pp.075505-1-075505-5, 2023-07-28. 応用物理学会
バージョン：

QUERY FORM

JOURNAL: Japanese Journal of Applied Physics

AUTHOR: M. Sakamoto et al.

TITLE: Improvement of the thermoelectric performance of boron-doped silicon by blocking minority carrier diffusion on the p^+/p interface

ARTICLE ID: ace4af

Page 1

Q1
Your article has been processed in line with the journal style. Your changes will be reviewed by the Production Editor, and any amendments that do not comply with journal style or grammatical correctness will not be applied and will not appear in the published article.

Page 1

Q2
The layout of this article has not yet been finalized. Therefore this proof may contain columns that are not fully balanced/ matched or overlapping text in inline equations; these issues will be resolved once the final corrections have been incorporated.

Page 1

Q3
IMPORTANT: This PDF reference document has been locked to prevent comments. Please use our online Proofing tool to answer all queries, make corrections and add comments.

Page 1

Q4
Please be aware that the colour figures in this article will only appear in colour in the online version.

Page 1

Q5
Please check that the **names of all authors as displayed in the proof are correct**, and that all **authors are linked to the correct affiliations**. Please also confirm that the correct corresponding author has been indicated. **Note that this is your last opportunity to review and amend this information before your article is published**.

Page 1

Q6
Please check that the funding information below is correct for inclusion in the article metadata.
Japan Society for the Promotion of Science: 21K04629, JP21K20489.

Page 1

Q7
We have been provided with ORCID iDs for the authors as below. Please confirm whether the numbers are correct.
Yuko Matsukawa 0000-0001-5664-8410

Page 5

Q8
If an explicit acknowledgment of funding is required, please ensure that it is indicated in your article. If you already have an Acknowledgments section, please check that the information there is complete and correct.

Page 5

Q9
Please check the details for any journal references that do not have a link as they may contain some incorrect information. If any journal references do not have a link, please update with correct details and supply a Crossref DOI if available.

Japanese Journal of Applied Physics **00**, 000000 (2023) **REGULAR PAPER**
https://doi.org/**10.35848/1347-4065/ace4af**

Improvement of the thermoelectric performance of boron-doped silicon by blocking minority carrier diffusion on the p^+/p interface

Momoka Sakamoto[1†‡], Yuko Matsukawa[2*†], Rikuto Sasaoka[2], Kohei Minoshima[2], Eisuke Nakamura[2], Arita Makoto[2], and Shinji Munetoh[2*]

[1]*Chikushigaoka High School, 2-13-1 Noma, Fukuoka 815-0041, Japan*
[2]*Department of Materials, Kyushu University, 744 Motooka, Fukuoka 819-0395, Japan*

[*]E-mail: matsukawa.yuko.357@m.kyushu-u.ac.jp; munetoh.shinji.599@m.kyushu-u.ac.jp
[†]These authors contributed equally to this work.
[‡]Present address: Department of Engineering, University of Washington, 3920 E. Stevens Way NE, Seattle, WA 98195, USA.

Received April 18, 2023; revised July 4, 2023; accepted July 4, 2023; published online MM DD, 2023

A two-layer bulk Si material with different boron concentrations was prepared using spark plasma sintering to improve its thermoelectric performance by blocking minority carrier diffusion across its interfaces. The sintered two-layer sample (p^+/p-Si) was cut to include the interface. Two monolayer samples (p^+-Si, p-Si) were prepared for comparison. Seebeck coefficient mapping of the p^+/p-Si surface by thermal probing confirmed a Seebeck coefficient gap between the two p-type Si layers, indicating that a band offset exists at the interface. When compared with the average resistivities and voltages for p^+-Si and p-Si, the electrical resistivity in the p^+/p-Si sample is almost identical, but the thermoelectric voltage is higher when the p^+-part is heated more than the p-part. This indicates that bipolar carrier transport inhibition in the band offset improved the thermoelectric voltage. This bandgap engineering process and principle can be extended to other thermoelectric materials that can be processed via powder sintering. © 2023 The Japan Society of Applied Physics

1. Introduction

In current internal combustion engines, 70% of the total energy generated from fossil fuels is lost in the form of waste heat at a temperature that generally exceeds 623 K via exhaust gases and the engine coolant.[1)] The use of thermoelectric power generation methods to reduce this energy waste is attracting considerable attention. Thermoelectric materials can semi-permanently convert heat into electrical power via the Seebeck effect without causing further CO_2 emissions.

Numerous studies have been devoted to the research and development of thermoelectric materials since the Seebeck effect was discovered in the 1800s. Bi–Te[2)] and Pb–Te[3)] systems are known to be promising thermoelectric materials in terms of their performance, but they contain expensive or toxic elements and are only available for operation in the low-temperature region; Bi_2Te_3 and PbTe-based materials have shown the highest values of the dimensionless figure of merit *ZT* at around 370 K[3)] and 870 K,[4)] respectively.[5)] Conventionally, many studies of thermoelectric materials have focused on the materials and chemical compositions that offer high Seebeck efficiency, but each material's shortcomings have hindered their practical application. Therefore, a novel method is required to make improvements in their thermoelectricity, regardless of the material type.

The bipolar effect degrades the thermoelectric voltage in materials with relatively narrow bandgaps.[6)] In the Seebeck effect in a p-type semiconductor, for example, charge separation is caused by diffusion of thermally generated holes from the high-temperature side to the low-temperature side of the material. However, at temperatures above 400 K, the electrons can be excited up to the conduction band (CB). The electrons then diffuse in the same direction as the holes in the valence band (VB) and suppress the charge separation process. Therefore, inhibition of the bipolar carrier transport can enhance the electric voltage in these materials. With this aim, approaches to optimize the band gaps and carrier concentrations by modifying the chemical compositions of the materials have been reported,[2,6–12)] although they are possibly restricted by doping limits and the trade-off with the electrical conductivity.[13,14)]

Another promising method for thermoelectric performance enhancement involves formation of interfaces in the material. Grain and compositional boundaries can increase the Seebeck coefficient via the carrier energy filtering effect and/or reduce the thermal conductivity via phonon scattering, and the coexistence or independence of these effects has also been discussed.[10,15–22)] The impact of grain boundaries and dopant segregation in polycrystalline Si results in higher resistivity, higher Seebeck coefficient, and lower thermal conductivity than in single crystalline Si, which has been under intense investigation for decades.[23–30)] The enhancement of *ZT* produced by heterostructure barriers in Bi_2Te_3, $Mg_2Sn_{1-x}Si_x$, $Si_{1-x}Ge_x$,[31)] and PbTe-based alloys[32)] have been investigated theoretically. Regarding experimental studies, there have been several reports on use of band bending to block minority carrier conduction and thus enhance the thermoelectric voltage. Growth of thin layers was demonstrated to realize an increase in the Seebeck coefficient due to minority carrier blocking.[33)] In bulk materials, research on functionally graded materials prepared via the Czochralski method implied that a composition gradient can improve the energy conversion efficiency[34)] and enable formation of an internal electric field that can control the diffusion of specific carriers.[35)] To enable this concept to be applied to other bulk materials, experimental demonstrations based on use of more common manufacturing methods, e.g. powder sintering, are desired.

In this study, two p-type semiconductors with different band structures are combined to form a band offset at their interface. We used Si as the model material because heavily doped Si has a narrower band gap than lightly doped Si.[36,37)] The band offset was fabricated by forming a junction composed of p-type Si layers with different carrier densities to inhibit diffusion of the excited electrons in the CB.

2. Experimental methods

2.1. Materials and preparation

Two types of boron-doped Si powder were sintered in two layers to form a p^+/p junction. The information on the degenerate and nondegenerate Si single crystals used as the raw materials is summarized in Table I.[36–38] The corresponding p^+-Si (degenerate) and p-Si (nondegenerate) ingots (>99% purity (SUMCO)) contain boron at concentrations of 3.0×10^{19} and 1.1×10^{19} cm^{-3}, respectively. When the Fermi levels (E_F's) of the p^+- and p-Si ingots are aligned, the bottom of the CB (E_{CB}) and E_F of the p^+-Si ingot is then estimated to be approximately 10 meV lower and 8 meV higher than the E_{CB} and top of the VB (E_{VB}) of the p-Si ingot, respectively. After pulverization to approximately 1 μm, these powders (9 g of each) were filled in layers into a carbon die with an inner diameter of 15 mm and combined via the spark plasma sintering method using a LABOX-215 (Sinter Land; 800 A and 3.0 V) for 10 min under vertical pressure of 50 MPa in a vacuum. A two-layered sample (p^+/p-Si) was cut to dimensions of 10 mm × 5.0 mm × 1.4 mm to include the interface at the center of its length. Hereafter, the part derived from the Si ingot doped with 3.0×10^{19} cm^{-3} of boron is called the p^+-part and the other, more lightly-doped part is called the p-part. For comparison, p^+-Si and p-Si monolayer samples were also prepared from 18 g of p^+-Si ingots and 18 g of p-Si ingots, respectively, using the same process that was used to form the p^+/p-Si sample. In addition, single-crystalline samples were also prepared by simply cutting each of p^+-Si and p-Si ingots, named p^+-sc-Si and p-sc-Si samples, respectively for comparison with the monolayer polycrystalline samples.

2.2. Characterization and measurement

X-ray diffraction (XRD) analysis using Cu Kα radiation was performed to characterize the crystal structure of the p^+/p-Si sample (SmartLab, Rigaku; 40 kV and 30 mA). The Seebeck coefficient distribution of the surface was examined by the thermal probe method using a probe that was heated to be 40 K higher than the stage at room temperature. The probe was in contact with the surface of a sample for more than 4 s to stabilize the temperature distribution inside the sample and render the heat transfer between the probe and the sample negligible. The probe diameter was around 50 μm and the scan step was set to 0.25 mm. The line profile of the voltage drop was scanned every 250 μm along the surface of each sample. For the p^+/p-Si sample, the current through the specimen from the p^+-part side to the p-part side was set at 100 mA to enable calculation of the resistivity of each part and the apparent resistivity of the entire scanned area. The p^+-sc-Si, p-sc-Si, p^+-Si, and p-Si samples were also scanned, although the p-Si sample was measured at a current of 50 mA. The thermoelectric voltages of the five samples were measured with a 3 K temperature difference between the edges of each sample. The results were calculated from two data sets measured by switching the direction of the temperature gradient for the sample setting location to eliminate any instrument bias. The p^+/p-Si sample produced two results that differed in the higher temperature part.

3. Results and discussion

3.1. Results

Figure 1 shows a photograph of the p^+/p-Si sample. The interface between the two different silicon layers cannot be observed clearly from the sample's visual appearance. The peaks of the diamond structure of Si alone were detected in the XRD pattern shown in Fig. 2.

Figure 3 shows mapping images of the Seebeck coefficients of (a) the p^+-Si sample, (b) the p-Si sample, and (c) the p^+/p-Si sample when investigated via the thermal probe method. The Seebeck coefficient was positive all around the scanned areas. Comparison of the two monolayer samples showed that the p-Si sample in Fig. 3(b) had higher coefficient values (expressed using darker colors) than the p^+-Si sample in Fig. 3(a). These results correspond to the fact that the p-Si ingot, which is the raw material for the p-Si sample, has a lower carrier concentration than the p^+-Si ingot used to form the p^+-Si sample, as listed in Table I. In Fig. 3(c), the left part (the p^+-part) is lighter in color than the right part (the p-part) of the p^+/p-Si sample. The sharp change in color corroborates the fact that an interface exists between the two Si layer types with different carrier concentrations, which can cause a rise in the E_{CB} at the boundary.

According to the line profile of the voltage drop, the resistivities of p^+-sc-Si, p-sc-Si, p-p^+-Si, and p-Si samples were determined to be 4.9, 8.8, 9.4, and 25 mΩ·cm, respectively. These results of the single crystalline samples are reasonable compared to the resistivity of silicon as a function of impurity concentration previously reported[39] and the polycrystalline sample showed higher resistivity than the corresponding single crystalline samples. Figure 4 shows the voltage drop across the p^+/p-Si interface, where the horizontal and vertical axes represent the position and the electric potential, respectively, with the origin set at a point near the p^+-part side. The slope changes noticeably at around 4 mm, which is the center of the sample. No significant voltage drop at this point indicates that there is no interface resistance between the two layers. The resistivities of the p^+-part, the p-part, and the complete sample (apparent value)

Table I. Information on the boron-doped Si single crystalline ingots used as the raw materials. The Fermi energies from the valence band edge ($E_{VB} - E_F$) and the apparent/net energy band gap narrowing (ΔE_g) near room temperature were derived from data and an equation published previously in the literature.[36–38]

Name	Dopant concentration (cm^{-3})	$E_{VB} - E_F$ (meV)	Apparent/net ΔE_g (meV)	Precursor to:
p^+-Si ingot	3.0×10^{19}	28	103	p^+-sc-Si sample (whole) p^+-Si sample (whole), p^+/p-Si sample (p^+-part)
p-Si ingot	1.1×10^{19}	−8	85	p-sc-Si sample (whole) p-Si sample (whole), p^+/p-Si sample (p-part)

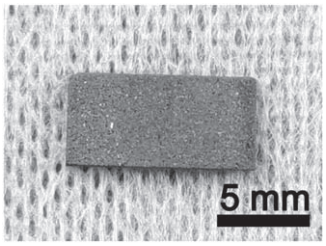

Fig. 1. Photograph of two-layer sample (p^+/p-Si) fabricated using the spark plasma sintering method. The left and right parts, called the p^+-part and the p-part, are derived from p^+-Si and p-Si ingots, respectively.

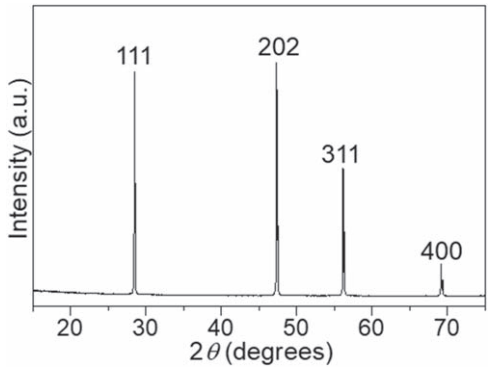

Fig. 2. XRD result for the p^+/p-Si sample. The numbers over the peaks are the indices of reflection of Si.

are 9.5, 22, and 15 mΩ·cm, as calculated from the solid, pointed, and dashed linear approximation lines shown in Fig. 4, respectively. Therefore, each of the different parts has similar characteristics to the p^+-Si or p-Si sample, and the complete sample characteristics are close to their average.

Figure 5 shows the temperature dependence of the thermoelectric voltages generated by the five samples with a 3 K temperature difference between their two edges. The potential of the low temperature part was plotted with reference to the potential of the high temperature part for each measurement. The Seebeck coefficients of p^+-sc-Si, p-sc-Si, p^+-Si, and p-Si were calculated from the voltages at 800 K to be 178, 213, 265, and 308 μV K^{-1}, respectively. The thermoelectric voltages in the single crystalline samples, lines (a) and (b) for the p^+-sc-Si and p-sc-Si samples, respectively, reproduced a monotonically increasing correlation within the measured temperature range, while these values are smaller than expected from those reported previously.[40] The reason for the higher resistivity and Seebeck coefficient in single-layer polycrystalline samples, lines (c) and (d) for the p^+-Si and p-Si samples, respectively, than in corresponding single crystalline samples may be explained as the result of energy filtering at grain boundaries.[41] The apparent Seebeck coefficient of the p^+/p-Si sample was 312 μV K^{-1} when the p^+-part side was hotter than the p-part side, although this value decreased to 221 μV K^{-1} with respect to the opposite temperature gradient. Note that we mention the *apparent* Seebeck coefficient for the p^+/p-Si sample as indicated by the *apparent* resistivity because these physical values should only be discussed for single-phase samples. Comparison of their temperature dependences showed that p^+-Si [line (c)] produced a lower thermoelectric voltage than p-Si [line (d)], which is consistent with the carrier concentrations of these precursors. The average of these values was plotted as the

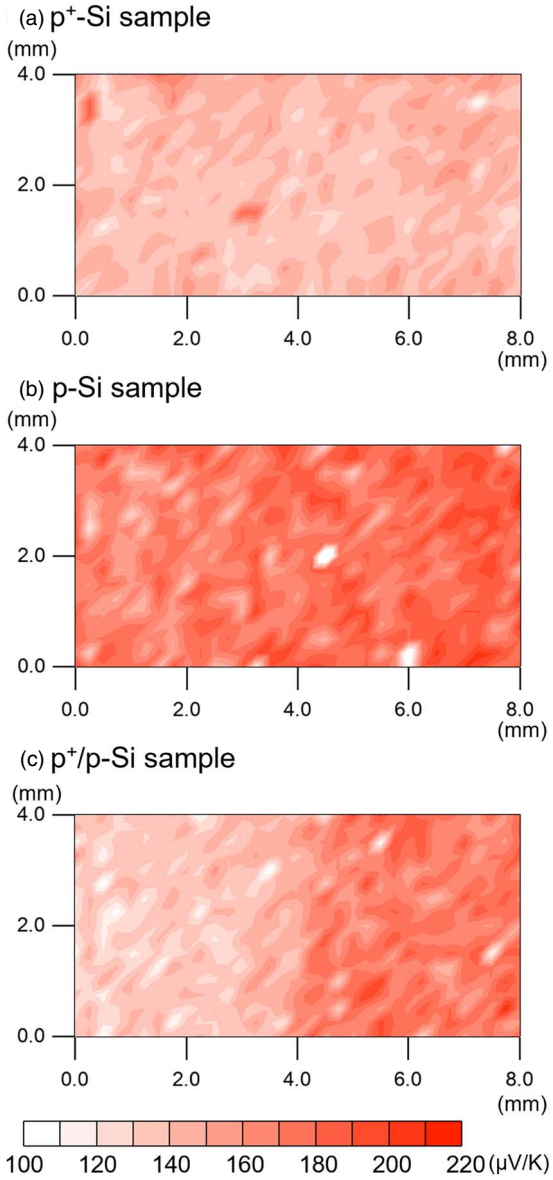

Fig. 3. Mapping images of the local Seebeck coefficients of (a) the p^+-Si sample, (b) the p-Si sample, and (c) the p^+/p-Si sample (where the left part is the p^+-part, and the right part is the p-part) acquired by the thermal probe method. The strength of the color corresponds to the magnitude of the Seebeck coefficient, as indicated by the color bar [see the legend below (c)].

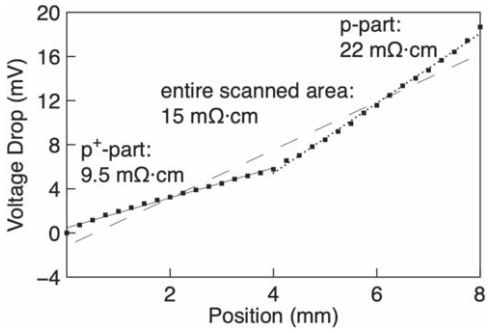

Fig. 4. Line profile of the voltage drop at a current of 100 mA for the p^+/p-Si sample (squares). Both the position and the voltage drop are referenced with respect to a point near the p^+-part-edge. Approximate straight lines for the p^+-part (solid), the p-part (pointed), and the entire sample (dashed) led to the corresponding resistivity values for these parts of 9.5, 22, and 15 (apparent value) mΩ·cm, respectively.

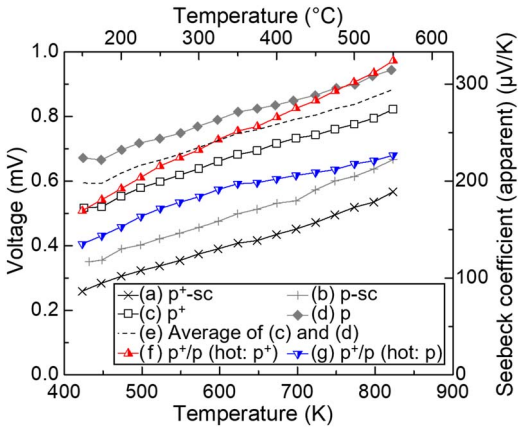

Fig. 5. Temperature dependence of the thermoelectric voltages of (a) the p^+-sc-Si sample, (b) the p-sc-Si sample, (c) the p^+-Si sample, (d) the p-Si sample, (e) the average of the data of the monolayer polycrystalline samples, and the p^+/p-Si sample (hot side: (f) p^+-part; (g) p-part) for a temperature difference of 3 K.

dashed line (e). When the p^+-part side was hotter than the other side, the thermoelectric voltage of the p^+/p-Si sample shown as line (f) was larger than the average voltages of the monolayer samples given by line (e), despite the coexistence of their high and low Seebeck coefficient layers, as shown in Fig. 3(c). In contrast, the result recorded under the switched temperature conditions [Fig. 5(g)] was lower than that of p^+-Si in addition to the average value. These phenomena can be caused by the obstruction and promotion of majority and minority carriers, which will be discussed in the next section.

3.2. Discussion

The p^+/p-Si sample has shown a thermoelectric voltage that differs from the average of the voltages of the monolayer samples, depending on the temperature gradient (Fig. 5). Regarding the distributions of the Seebeck coefficient and the resistivity (Figs. 3 and 4), the p^+/p-Si sample has characteristics similar to a combination of the p^+-Si and p-Si characteristics. Therefore, the existence of the interface at the p^+/p-Si junction should be the reason why the thermoelectric voltage of the p^+/p-Si sample [Figs. 5(f) and (g)] is different from the average of the values for p^+-Si and p-Si [Fig. 5(e)]. This is explained schematically in Fig. 6. As indicated within Table I, when semiconductors derived from p^+-Si and p-Si are joined together, an E_{CB} slope with a rise of 10 meV and a gap between E_F of p^+-part and E_{VB} of p-part with a fall of 8 meV will be formed at their interface [as shown in Fig. 6(a)]. This band bending structure prevents electrons, which were excited preferentially at the p^+-part from diffusing into the CB in the p-part, as shown in Fig. 6(b). Simultaneously, the corresponding hole diffusion is also inhibited in the VB. This offset can severely inhibit hole diffusion especially in the low temperature range, resulting in the lower thermoelectric voltage for p^+/p-Si sample (hot side: p^+-part) [Fig. 5(f)] than that for the average of the values for monolayered polycrystalline samples [Fig. 5(e)]. On the other hand, when the temperature range is increased, the electrons cannot cross the 10 meV offset as easily as the holes can cross the 8 meV offset, and this results in effective charge separation [Fig. 6(c)]. Therefore, the band offset can contribute to the improvement in the thermoelectric voltage. However, when the temperature gradient is switched (hot side: p-side), the thermoelectric voltage of the p^+/p-Si sample [Fig. 5(g)] is even lower than that of the p^+-Si [Fig. 5(c)] over the entire temperature range. In that case, both of majority and minor carries may easily diffuse to the p^+ side as shown schematically in Fig. 6(d), resulting in recombination and voltage drop in that sample. The validity of use of this artificially modified band structure to eliminate the bipolar effect was confirmed in addition to the polycrystallization in this study.

To discuss the performance in a useful manner, the p^+/p-Si sample must be compared with the p-Si sample. Although the voltage across the p^+/p-Si sample [hot side: p^+-part, Fig. 5(f)] was initially lower than that of the p-Si sample [Fig. 5(d)], the voltages were almost the same at temperatures above 750 K. In addition, the entire apparent resistivity of p^+/p-Si (15 mΩ·cm) was lower than the resistivity of p-Si (25 mΩ·cm). Therefore, it can be concluded that the junction composed of p-type Si layers with different carrier densities can achieve higher thermoelectric performances than the conventional monolayered structures.

4. Conclusions

The thermoelectric voltage of boron-doped Si is improved by forming a junction from two boron-doped Si parts with different band structures that are dependent on their dopant concentrations. This result indicated that a band offset was formed at the interface that can inhibit diffusion of excited

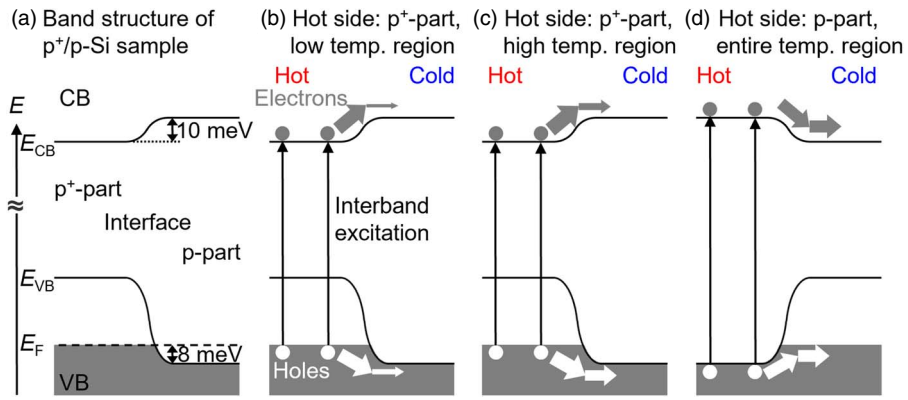

Fig. 6. Schematic illustrations of (a) the band structure, the mechanism by which diffusion of excited electrons from the valence band (VB) to the conduction band (CB) and the corresponding holes are inhibited by offsets in the CB and VB, respectively in (b) low and (c) high temperature regions when the p^+-part is heated more than the p-part, and (d) that in entire temperature region when the p-part is heated more than the p^+-part of the p^+/p-Si sample.

electrons in the CB. The larger charge separation caused by the barrier with respect to the minority carriers can contribute an increase in the electric voltage across the two-layered thermoelectric material, which is prepared by powder sintering.

Q8

Acknowledgments

This work was supported by Japan Society for the Promotion of Science (JSPS) KAKENHI Grants-in-Aid for Young Scientists (Start-up) under Grant Number JP21K20489 for Y.M. and for Scientific Research (C) under Grant Number 21K04629 for M.A. M.S. would like to thank the Kyushu University Future Creators in Science Project (AY2020). The authors wish to thank Kosuke Aoki and Takuto Kumakawa (Kyushu University) for their development of a procedure that allowed samples to be sintered with good reproducibility. We thank David MacDonald, MSc, from Edanz (https://jp.edanz.com/ac) for editing a draft of this manuscript.

ORCID iDs

Yuko Matsukawa https://orcid.org/0000-0001-5664-8410

Q9

1) Z.-G. Shen, L.-L. Tian, and X. Liu, Energy Convers. Manag. **195**, 1138 (2019).
2) H. Cho, H. Kim, M. Kim, K. H. Lee, S. W. Kim, and S. Kim, J. Electron. Mater. **49**, 2789 (2020).
3) B. Poudel et al., Science **320**, 634 (2008).
4) Q. Zhang, F. Cao, W. Liu, K. Lukas, B. Yu, S. Chen, C. Opeil, D. Broido, G. Chen, and Z. Ren, J. Am. Chem. Soc. **134**, 10031 (2012).
5) S. Chen and Z. Ren, Mater. Today **16**, 387 (2013).
6) L. Chen et al., Mater. Today Phys. **21**, 100544 (2021).
7) H. Zhu, J. Luo, H. Zhao, and J. Liang, J. Mater. Chem. A **3**, 10303 (2015).
8) Y. Xiao et al., J. Mater. Chem. A **2**, 20288 (2014).
9) Z. Guo, K. Song, Z. Yan, P. Sun, X. Tan, G. Wu, Q. Zhang, G.-Q. Liu, B. Yu, and J. Jiang, Chem. Eng. J. **426**, 131853 (2021).
10) H. Wu et al., Energy Environ. Sci. **8**, 3298 (2015).
11) X. Luo, M. B. Sullivan, and S. Y. Quek, Phys. Rev. B **86**, 184111 (2012).
12) J. Zhang et al., Nat. Commun. **2**, 574 (2011).
13) Y. Xiao et al., Adv. Energy Mater. **9**, 1900414 (2019).
14) L.-D. Zhao et al., J. Am. Chem. Soc. **135**, 7364 (2013).
15) P. Puneet, R. Podila, M. Karakaya, S. Zhu, J. He, T. M. Tritt, M. S. Dresselhaus, and A. M. Rao, Sci. Rep. **3**, 3212 (2013).
16) C. Zhang, H. Ng, Z. Li, K. A. Khor, and Q. Xiong, ACS Appl. Mater. Interfaces **9**, 12501 (2017).
17) Y. Li, X. Wang, G. Liu, B. Shin, and F. Shan, Scr. Mater. **172**, 88 (2019).
18) J. Hwang et al., ACS Nano **13**, 8347 (2019).
19) M. Bachmann, M. Czerner, and C. Heiliger, Phys. Rev. B **86**, 115320 (2012).
20) K. Biswas, J. He, I. D. Blum, C.-I. Wu, T. P. Hogan, D. N. Seidman, V. P. Dravid, and M. G. Kanatzidis, Nature **489**, 414 (2012).
21) J. Yang, L. Xi, W. Qiu, L. Wu, X. Shi, L. Chen, J. Yang, W. Zhang, C. Uher, and D. J. Singh, NPJ Comput. Mater. **2**, 15015 (2016).
22) S. Kim, K. Y. Lee, and J.-H. Lim, Materials **13**, 2835 (2020).
23) J. Y. W. Seto, J. Appl. Phys. **46**, 5247 (1975).
24) X. Zianni and D. Narducci, Nanoscale **11**, 7667 (2019).
25) G. Schierning, Phys. Status Solidi A **211**, 1235 (2014).
26) D. Narducci, S. Frabboni, and X. Zianni, J. Mater. Chem. C **3**, 12176 (2015).
27) X. Zianni and D. Narducci, J. Appl. Phys. **117**, 035102 (2015).
28) X. Zianni and D. Narducci, Mater. Today Proc. **8**, 706 (2019).
29) C. H. Seager, Ann. Rev. Mater. Sci. **15**, 271 (1985).
30) T. I. Kamins, J. Appl. Phys. **42**, 4357 (1971).
31) J.-H. Bahk and A. Shakouri, Phys. Rev. B **93**, 165209 (2016).
32) J.-H. Bahk and A. Shakouri, Appl. Phys. Lett. **105**, 052106 (2014).
33) P. G. Burke, B. M. Curtin, J. E. Bowers, and A. C. Gossard, Nano Energy **12**, 735 (2015).
34) Z. Dashevsky, S. Shusterman, M. P. Dariel, and I. Drabkin, J. Appl. Phys. **92**, 1425 (2002).
35) Y. Osakabe, S. Tatsumi, Y. Kotsubo, K. Yamasoto, S. Munetoh, O. Furukimi, and K. Nakashima, J. Functionally Graded Mater. **33**, 8[in Japanese] (2019).
36) S. C. Jain and D. J. Roulston, Solid State Electron. **34**, 453 (1991).
37) J. W. Slotboom and H. C. de Graaff, Solid State Electron. **19**, 857 (1976).
38) W. P. Dumke, J. Appl. Phys. **54**, 3200 (1983).
39) J. C. Irvin, Bell Syst. Tech. J. **41**, 387 (1962).
40) Y. Ohishi, J. Xie, Y. Miyazaki, Y. Aikebaier, H. Muta, K. Kurosaki, S. Yamanaka, N. Uchida, and T. Tada, Jpn. J. Appl. Phys. **54**, 071301 (2015).
41) D. Narducci, E. Selezneva, G. Cerofolini, S. Frabboni, and G. Ottaviani, J. Solid State Chem. **193**, 19 (2012).